Transactions of the SMiRT 27
Yokohama, Japan, March 3-8, 2024
Division V

NONLINEAR STRUCTURE SSI ANALYSIS STUDY FOR RC BUILDING ON SOIL SITE IN TOKYO AREA PER JEAC 4601 RECOMMENDATIONS

Dan M. Ghiocel[1], Yasuo Nitta[2] and Ryosuke Ikeda[3] and Tomohiro Horiguchi. [4]

[1] President, Ghiocel Predictive Technologies, Inc., New York, USA (dan.ghiocel@ghiocel-tech.com)
[2] Senior Engineer, SHIMIZU Corporation, Tokyo, Japan (nitta_y@shimz.co.jp)
[3] General Manager, SHIMIZU Corporation, Tokyo, Japan (ikedar@shimz.co.jp)
[4] Structural Engineer, Terrabyte Corporation, Tokyo, Japan (tomohiro.horiguchi@terrabyte.co.jp)

ABSTRACT

The paper investigates the seismic SSI effects for a typical Auxiliary Building (AB) shearwall surface structure founded on a soft soil deposit under coherent and incoherent seismic soil motions. The site-specific condition corresponds to the Chiba city in Tokyo area. Seismic input was defined by the standard design response spectra (DRS) used for non-nuclear, conventional civil structures based on the Japan seismic intensity map. The seismic input was applied at a depth that is defined at the top of a stiff soil layer formation with a Vs above 400 m/s which is at -24m depth for the Chiba site soil layering. The motion incoherency was modeled based on the Chiba site dense-array records. The nonlinear structure SSI analysis follows the JEAC 4601 and AIJ RC recommendations for reinforced concrete (RC) structure modeling applied to the detailed 3DFEM of the AB structure. The SSI analysis was based on an efficient iterative hybrid approach which couples the equivalent-linear overall SSI analysis in complex frequency-domain with a nonlinear superstructure analysis in time-domain. The nonlinear SSI approach was implemented in the ACS SASSI Option NON software. Comparative results indicate that incoherent motions produce larger structural stress-dependent stiffness degradations in the RC walls than coherent motions. This effect is produced by the large incoherent-induced kinematic SSI effects generated by the non-vertically propagating seismic wave differential soil motions that increase the foundation mat deformation and stresses.

AB STRUCTURE SSI MODEL AND SEISMIC SITE-SPECIFIC CONDITIONS

The AB structure is a shearwall structure with a significant mass eccentricity. This structure was selected on purpose to be a sensitive design to the torsional motion. Figure 1 shows the AB elastic linear structure model, while Figure 2 shows the nonlinear structure model. Figure 2 shows the assigned RC wall concrete nonlinear materials which have different colours for the RC wall webs and flanges. The flange widths were computed in accordance with the JEAC 4601-2015 and AIJ RC-2018 standard requirements. The variation of flange widths with height is due to the wall different clearances.

The seismic standard design response spectra (DRS) for horizontal and vertical directions, and the Chiba site soil layering Vs profile is shown in Figures 3 and 4. The nonlinear soil behaviour was modelled based on the experimental soil constitutive stiffness and damping curves as functions of soil shear-strain as shown in Figure 5. The standard DRS is input at – 24m depth that corresponds to the top of the stiffer soil formation with a Vs = 420 m/s (see orange arrow in Figure 4). Figure 6 shows in upper plots the seismic outcrop DRS input and its spectrum compatible acceleration time history in horizontal direction, and in lower plots the surface ground response spectra (GRS) and soil acceleration motion. Figure 6 indicates that the seismic ground surface GRS has significantly frequency content with large amplitudes above 1.5g, for broad frequency range from about 1.5 Hz to 10 Hz. It should be noted that the 1.5 Hz-10 Hz frequency range corresponds to seismic waves with wavelengths (= Vs/f) varying between 15 m and 100 m in the upper soil layers which can affect the AB foundation motion as explained in this section.

The ground surface was computed using the SHAKE approach for (iterated soil using 1D vertical seismic wave propagation). The in-column soil motion at -24 depth is also shown in the lower left plot. The iterated Vs profile vs. the initial, low-strain Vs profile is shown in Figure 7.

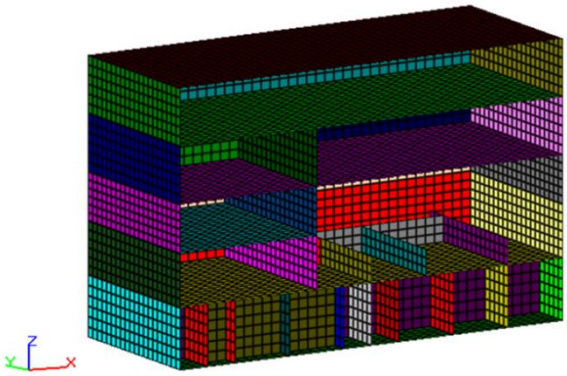

Figure 1 AB Shearwall RC Structure Model

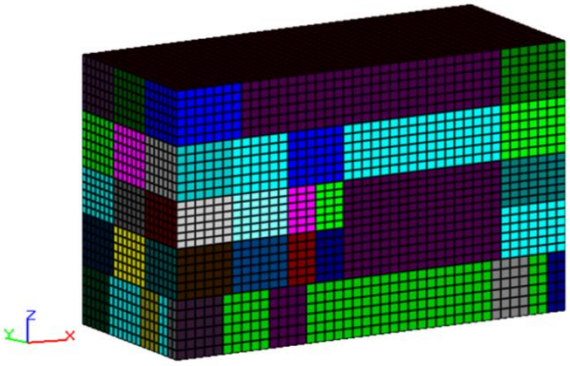

Figure 2 AB Structure RC Wall Materials

Horizontal Direction:

$$S_{a0}(T,0.05)=\begin{cases}a_0(1+9.375T) & (T\le 0.16)\\ 2.5a_0 & (0.16<T<0.64)\\ 1.6a_0/T & (T\ge 0.64)\end{cases}$$

Vertical Direction

$$S_{av}(T,0.05)=\begin{cases}a_0(1+9.375T)\times 20/31 & (T<0.1)\\ 2.5a_0\times 1/2 & (0.1\le T<0.64)\\ 1.6a_0/T\times 1/2 & (T\ge 0.64)\end{cases}$$

Figure 3 Seismic Standard Design Spectra in Japan

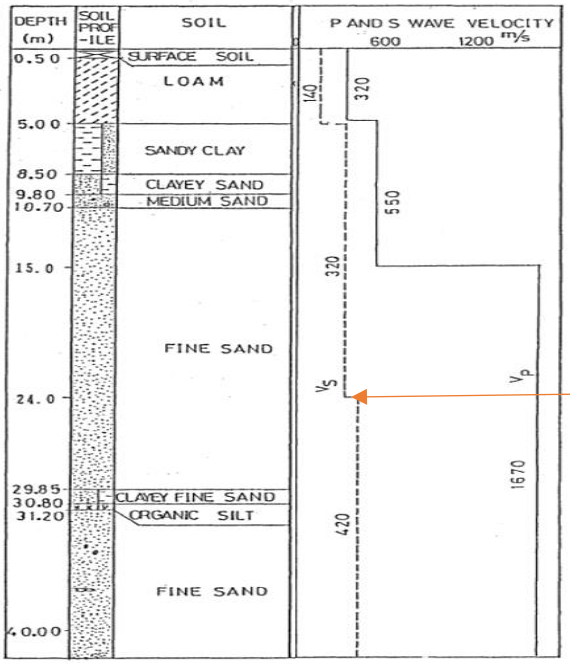

Figure 4 Chiba Site Soil Layering Vs Profile

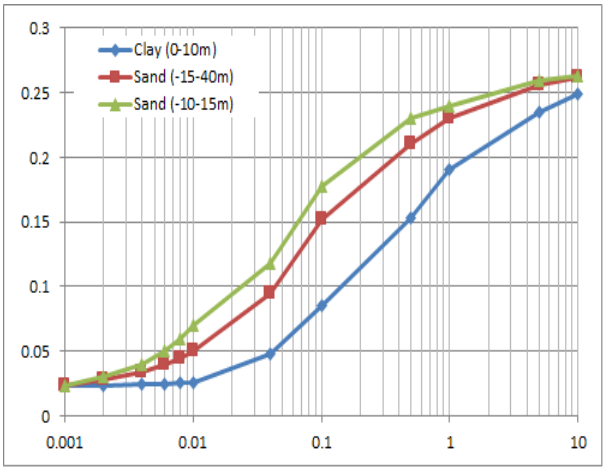

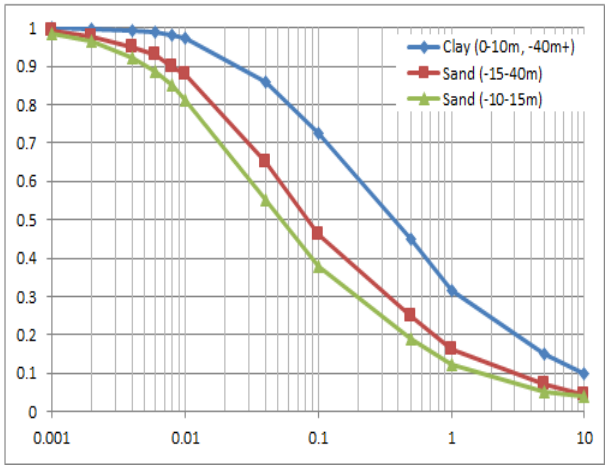

Figure 5 Soil Material Curves; Damping (left) and Shear Modulus (right), Functions of Soil Shear Strain

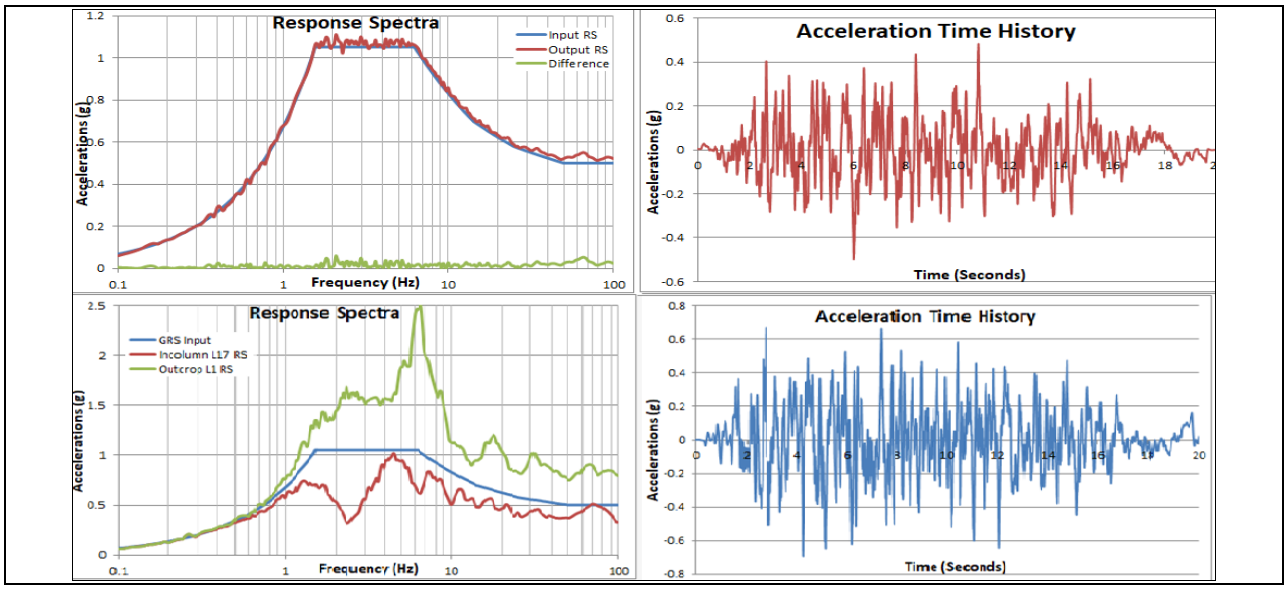

Figure 6 -24m Depth Input DRS (upper left) and Computed Surface GRS (lower left, green) and Associated Acceleration Time Histories (right), Plus In-Column GRS at -24m Depth (lower left, red)

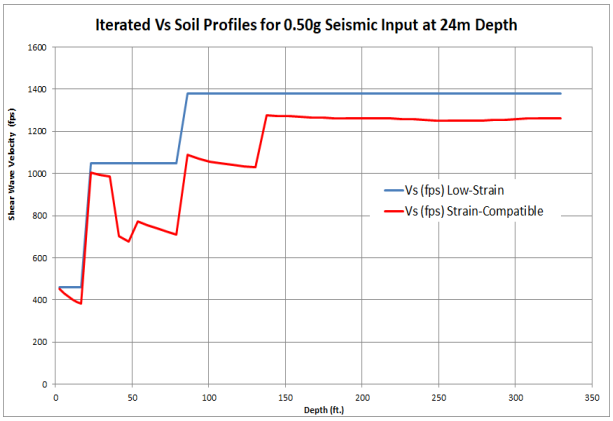

Figure 7 Low-strain vs. Effective Strain Vs Profile

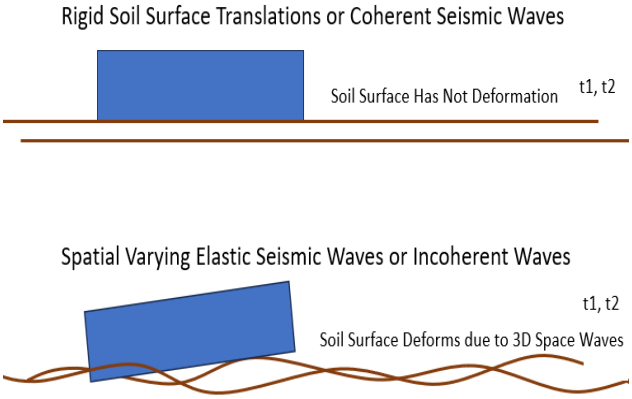

Figure 8 Coherent vs. Incoherent Soil Motion Effects

Figure 8 illustrates a qualitative comparison between the coherent (1D motion) and the incoherent (3D motion) seismic soil motions. If the seismic wave wavelengths are equal or less than the foundation sizes, then, the elastic soil waves will affect the foundation motion due to the differential soil motions which are applied simultaneously to the foundation mat. This is the AB structure case which has a foundation area of 60m x 25m. The AB structure on soft soil deposit, basically behaves as a multiple-support excited structure; with both soil acceleration and soil relative displacements being simultaneously applied to foundation. These differential motions produced by seismic soil motion spatial variation in horizontal plane, due to random incident inclined body waves and surface waves may affect the foundation deformation.

It should be noted that the structural design codes which are based on the ultimate state limit for the RC structures do not include the structure support deformation effects which produce the secondary stresses, except for some special situations, as for example, for the large-span highway bridges. This is a potential engineering pitfall as shown in next section.

Figure 9 shows a three-dimensional view sketch of the soil surface motion under coherent and incoherent seismic waves. Incoherent motions correspond to realistic dense-array recorded seismic waves including a mix of inclined body and surface waves with random contributions. Abrahamson considered that incoherency is generated in the soil layers above the 500 m depth (Abrahamson, 2007). Also, the

Abrahamson coherence functions for soil and rock sites indicate that the motion incoherency is much larger for soft soil deposits than for hard soil or rock formations due to the low speed of seismic waves in the soft soils (Figure 10). These soft soil seismic waves have much shorter wavelengths which can be a fraction of the size of a large-size building foundation, as apparent could happens for AB structure on the Chiba soft soil site.

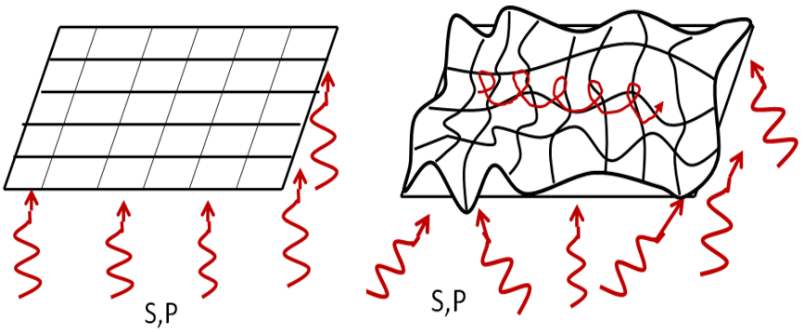

Figure 9 1D Coherent (left) vs. 3D Incoherent (right) Soil Motions

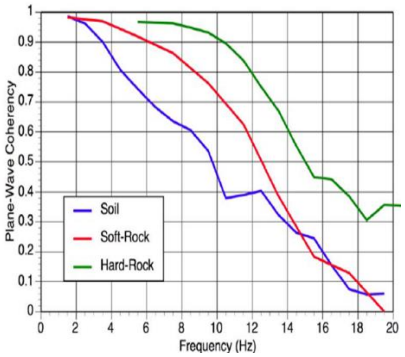

Figure 10 Soil and Rock Coherence

Based on the many earthquake motions recorded by the Chiba dense array, the coherence function for the Chiba soil site was determined (Katayama et al, 1990). The Chiba coherence function is shown in Figure 11. The mean values were used for the five coefficients: C0=0.0306, C1=57,850, C2=88.8, C3=46 and C4=1.07. It should be noted the relative isotropic distances were used in the coherence analytical expression, computed as the length computed based on the radial and tangential relative distances which were used for the Chiba circular-shaped dense array.

$$\gamma_{jj}(\xi_r, \xi_t, f) = e^{-c_0 f} \exp\left(-\frac{f^2 + {c_3}^2}{{c_1}^2}\xi^2\right) + \left(1 - e^{-c_0 f}\right)\exp\left(-\frac{f^2}{{c_2}^2}\xi^2\right)$$

$$\xi^2 = {c_4}^2 {\xi_r}^2 + {\xi_t}^2$$

Figure 11 Chiba Soil Site Coherence Function Determined Based on Many Seismic Records

Figure 12 shows a comparison between Chiba soil site and Abrahamson soil and rock site coherence functions.

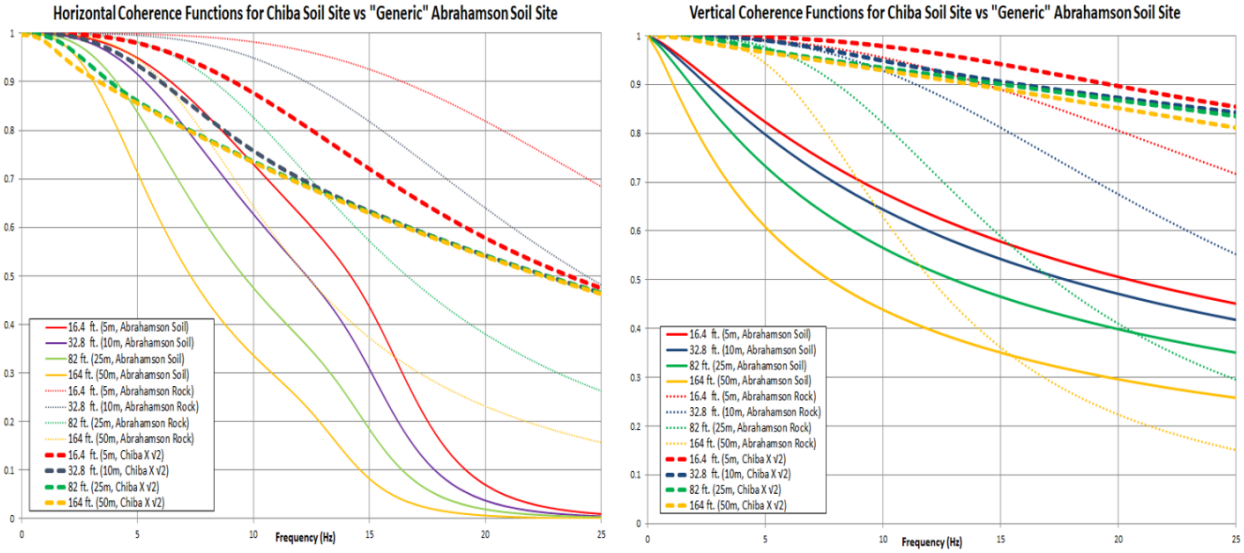

Figure 12 Chiba Site vs. Abrahamson Coherence Functions for Horizontal (left) and Vertical (right) Axes

The differences in the high frequency are assumed to be due to the different definitions of the two types of coherence functions. It should be noted that the Abrahamson functions are plane-wave coherences which go faster down to a zero-value at higher frequencies than the China site lagged coherences. However, in the lower frequency range of 2-10 Hz the values are much closer. Additional investigations are required to clarify the differences in the coherence function decays in the high frequency for the two coherences.

2. NONLINEAR STRUCTURE SSI ANALYSIS PER JEAC 4601-2015 STANDARD

For the AB structure RC walls, the structural modelling was based on the JEAC 4601 recommendations. The RC wall back-bone curve (BBC) equations for the nonlinear SSI analysis were computed using the JEAC 4601 Appendix 3.7 equations. The RC wall nonlinear modelling included two major constitutive components (Figure 13):

1. Back-bone curves (BBC) for shear and bending deformation for each RC wall at each floor level per JEAC 4601 App. 3.7 equations or available experimental tests (left plot, red curve)

2. Hysteretic models (HM) for the shear and bending cyclic deformation effects for each RC wall panel, selected per JEAC 4601 standard recommendations or available experimental tests (left plot, blue loops)

The RC wall BBCs and their associated hysteretic models were determined using ACS SASSI Option NON based on the requirements of the JEAC 4601-2015 App.3.7. Therefore, the "PO shear" and "PODT bending" hysteretic models recommended by the standard were used for the nonlinear structure SSI analysis are the maximum point-oriented models shown in Figure 13, right plots. These hysteretic models are included in the Option NON hysteretic model library.

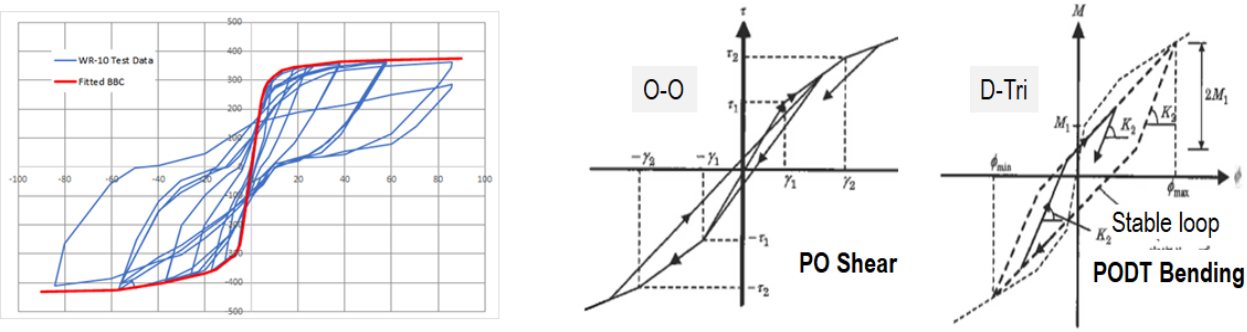

Figure 13 BBC and JEAC 4016 Recommended Maximum Point-Oriented Hysteretic Models

For nonlinear structure SSI analysis, an iterative hybrid frequency-time approach was used for performing an efficient nonlinear structure SSI analysis. The hybrid approach includes at each iteration two coupled analysis steps (Figure 14):

Step 1: Perform an *equivalent-linear SSI analysis* in complex frequency via the SASSI approach to compute the structural displacements for each nonlinear RC wall, and then,

Step 2: Perform a *nonlinear time-domain hysteretic analysis* for each RC wall loaded with the SSI displacements from Step 1, to compute the in-plane shear and bending nonlinear wall responses using the *standard-based back-bone curve (BBC) equations* and the *appropriate hysteretic models from the available software library*.

It should be noted that *Step 1* uses the *original, refined FE SSI model* (left plot) while *Step 2* uses a *reduced-order structural model* (right plot) using macro-mechanics models for simulating the RC wall hysteretic behaviour. These macro-mechanics models are called wall panels and include all groups of the shell elements defining the RC wall geometry at each floor level (see wall panels in different colours in Figure 9 left plot). Therefore, the Step 2 "true" nonlinear time-domain hysteretic analysis is extremely fast.

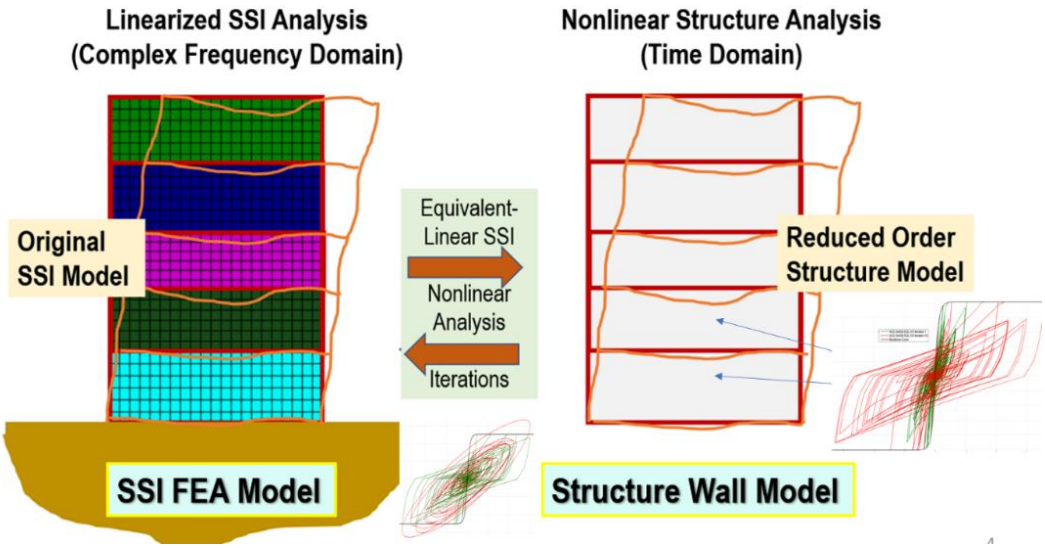

Figure 14 Fast Iterative Hybrid Nonlinear SSI Approach Implemented in ACS SASSI NON

It should be noted that the ACS SASSI Option NON was developed in compliance with the US and Japan standards for nonlinear modelling of the RC and SC structures (Ghiocel et al. 2022a, 2022b). Independent verification and validation studies against experimental testing and other sophisticated nonlinear time domain FEA codes indicated that the iterative SSI equivalent-linearization procedure implemented in the ACS SASSI Option NON provides a reasonable accuracy and a high numerical efficiency (Nitta at al., 2022 Ichihara et al., 2022).

AB STRUCTURE RC WALL NONLINEAR MODELING PER JEAC 4601-2015 STANDARD

The first step for the nonlinear RC structure modeling is to identify the main resistance RC walls which are assumed to have behave nonlinearly during the earthquake. For these RC walls, nonlinear FE submodels need to be defined as shown in Figure 15 for the AB structure.

The AB structure includes nine nonlinear wall submodels. For each nonlinear wall submodel, at each floor level, the subdivisions of the walls per floor level are defined as wall panels. As shown in Figure 14, these wall panels are numbered bottom-up in a sequential order. Each plane RC wall includes in its cross-section the wall web and the two flanges. The wall flange widths are computed in accordance with the JEAC 4601-2015 and AIJ RC-2018 requirements. For regular RC walls with planar webs, it should be noted that the nonlinear material degradation is different in the wall webs and wall flanges since the web damage is governed by the in-plane shear deformation and the flange damage is governed by the bending deformation (as colored in Figure 2).

If orthotropic materials are defined for flanges, then, at each iteration, the interactive bending and shear damage effects can be incorporated into a single physical material model with decoupled shear and bending stiffnesses. Figure 16 shows the shear and bending BBC computed for the exterior RC wall, namely, the Wall 1 submodel.

For the nonlinear structure SSI analysis, the “PO shear” and “PODT bending” hysteretic models were used for modeling the RC wall panel behavior under the seismic random load time history variations.

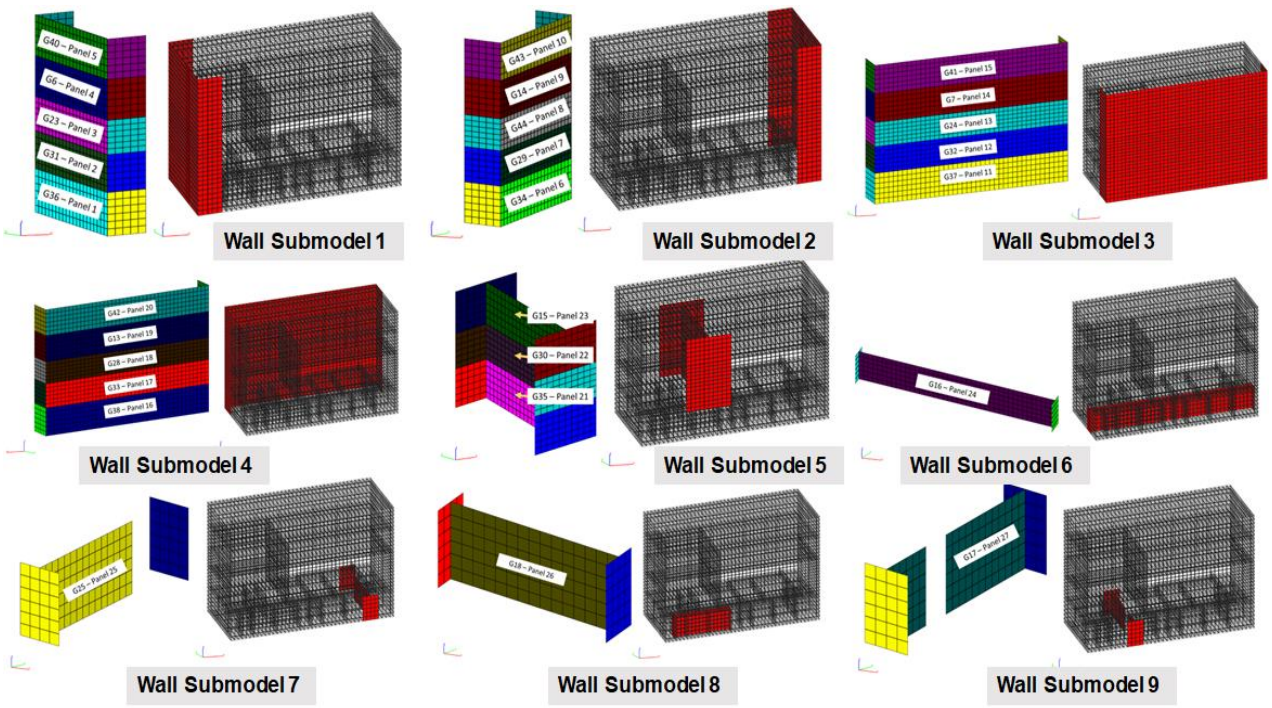

Figure 15 The AB Structure RC Wall Nonlinear Submodels (5 Submodels 1,2,5,7,9 for Transverse Direction, and 4 Submodels 3,4,6,8 for Longitudinal Direction)

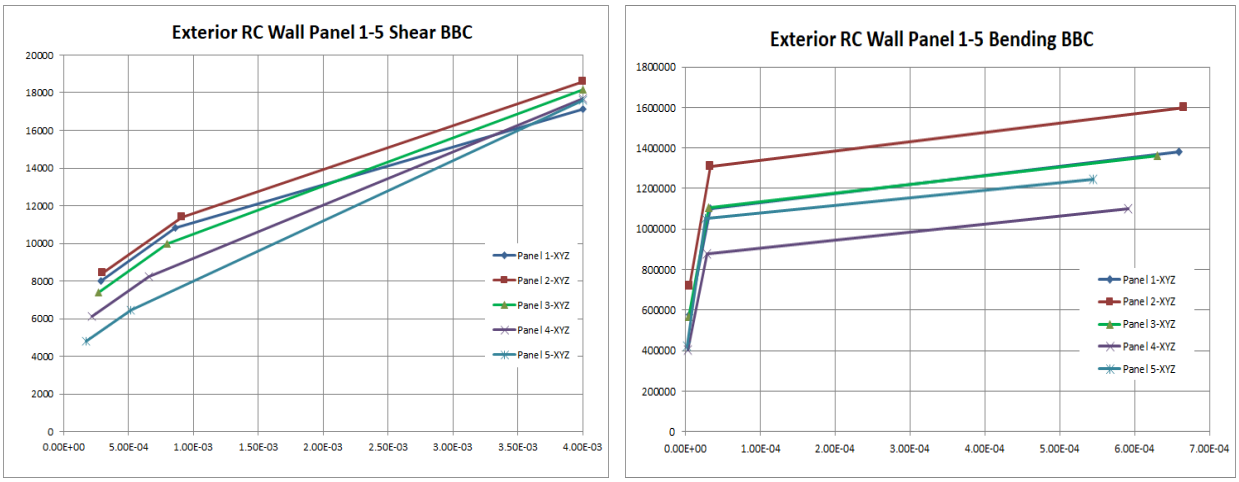

Figure 16 Shear and Bending BBC for Exterior RC Wall 1 Panels (5 Floor Levels, Panels 1-5)

4. COMPARATIVE SSI ANALYSIS RESULTS

To evaluate the AB nonlinear SSI structure responses for coherent and incoherent seismic wave inputs, acceleration in-structure response spectra (ISRS) and structure accelerations and displacements were computed. Figure 16 shows a comparison of the linear and nonlinear ISRS at top of AB structure for both coherent (green lines) and incoherent motions for Abrahamson coherence (blue lines), and the Chiba coherence (red lines). As expected, the nonlinear ISRS amplitudes a\were significantly lower than the linear ISRS amplitudes for both coherent and incoherent inputs It should be also noted that using the two coherence functions does not visibly change the ISRS responses. Figure 17 shows that the nonlinear incoherent ISRS are lower than the nonlinear coherent ISRS, especially for the longitudinal direction.

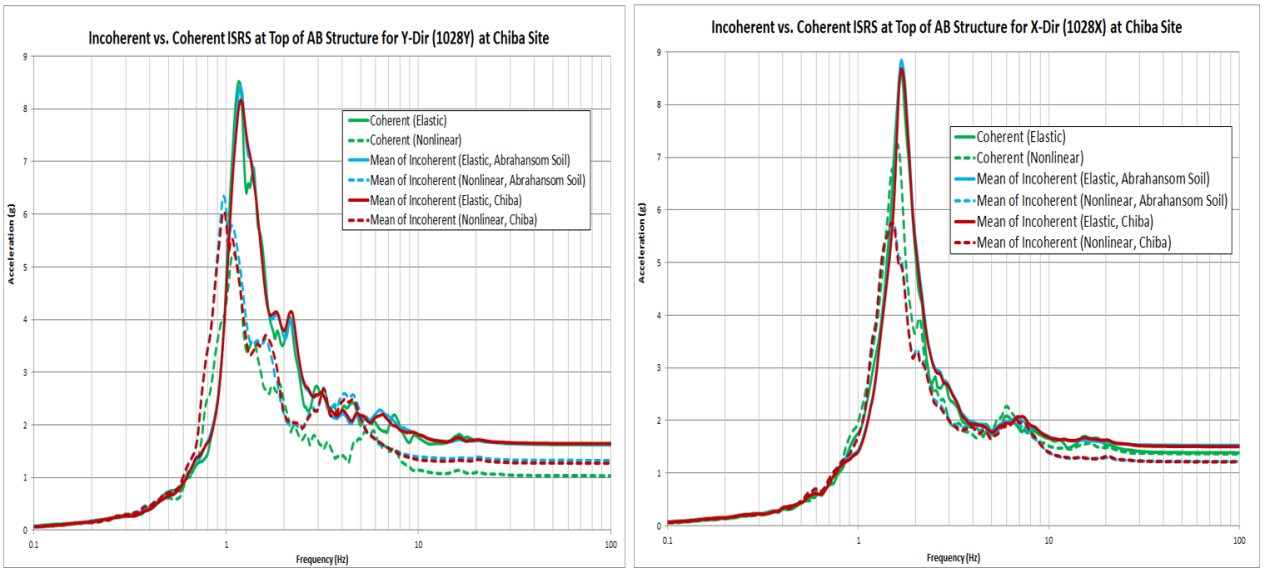

Figure 17 Coherent and Incoherent ISRS at Top of AB Structure for X and Y Directions

Figure 18 shows the AB structural (highly scaled) instant displacements the same time step computed for coherent and incoherent motions. It should be noted that at the selected time instants, the foundation baseslab is significantly bent under the incoherent wave motion. The short wavelength incoherent soil waves impinge the AB foundation baseslab to follow the soil deformation under these simulated 3D random incoherent waves. Although, the soil wave displacement amplitudes are very small, they could largely affect the stresses in the stiff foundation baseslab.

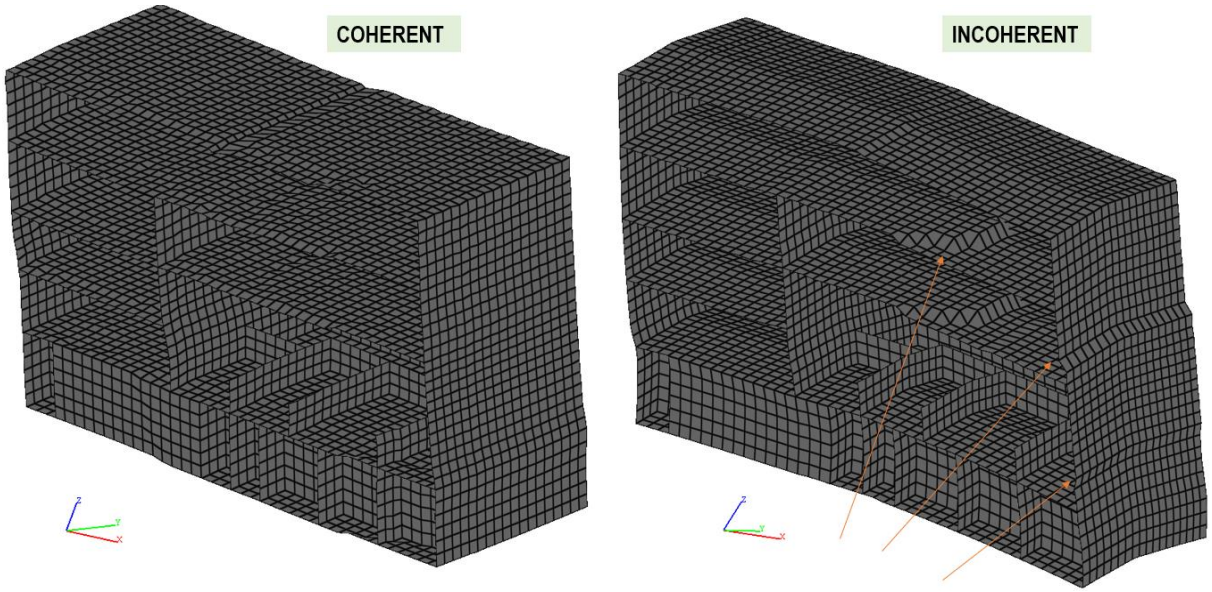

Figure 18 AB Structure Scaled Displacements at Same Time Step Under Coherent and Incoherent Inputs

Figure 19 shows the AB foundation baseslab instant displacement under coherent and incoherent seismic waves based on Chiba coherence function. It is obvious that the short wavelength seismic incoherent waves bent visibly the AB structure baseslab in both the X and Y directions.

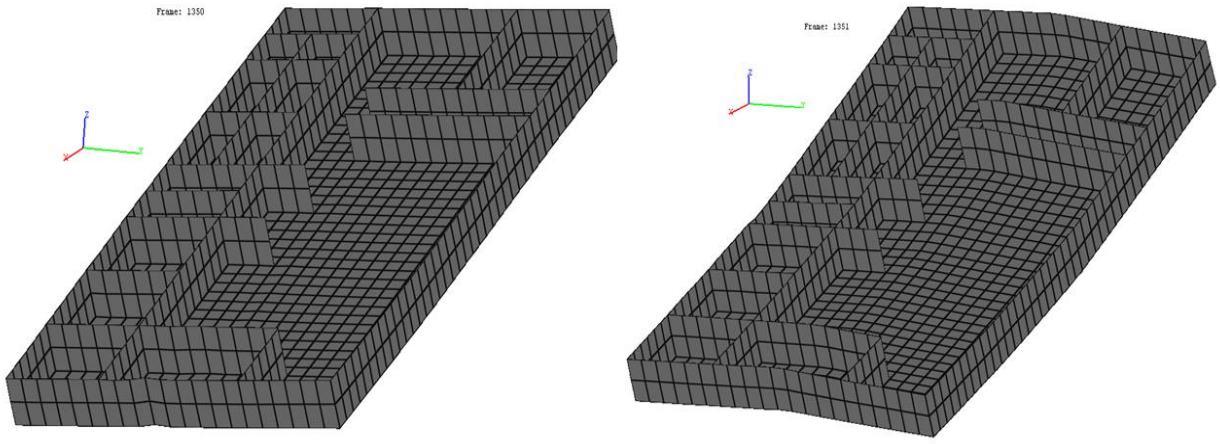

Figure 19 AB Structure Baseslab Instant Displacements Under Coherent and Incoherent Inputs

Incoherent motion waves also excite the torsional vibration motion of the entire AB structure that has a large mass eccentricity. Figure 19 compares the ISRS at the AB top corner for the transverse and longitudinal directions. In X-longitudinal direction, under coherent input the nonlinear ISRS dominant spectral peak at 1.8 HZ is much larger than for incoherent input (7.2 versus 5.8). In contrast, in Y-transverse direction, under coherent input, the nonlinear ISRS dominant spectral peak at 1.2 HZ is much smaller than for incoherent input (5.2 versus 6.2). This indicates that incoherent motion produces a more uniform shear deformation in the RC walls due to the induced torsional motion.

In Figure 20 shows that as the result of the incoherency-induced torsional motion, the AB structure responses become more uniform for the two horizontal directions. Torsion significantly decreased the ISRS (and increased the shear deformation) for the longitudinal RC walls, and increased the ISRS (and decreased the shear deformation) for the transversal walls RC walls.

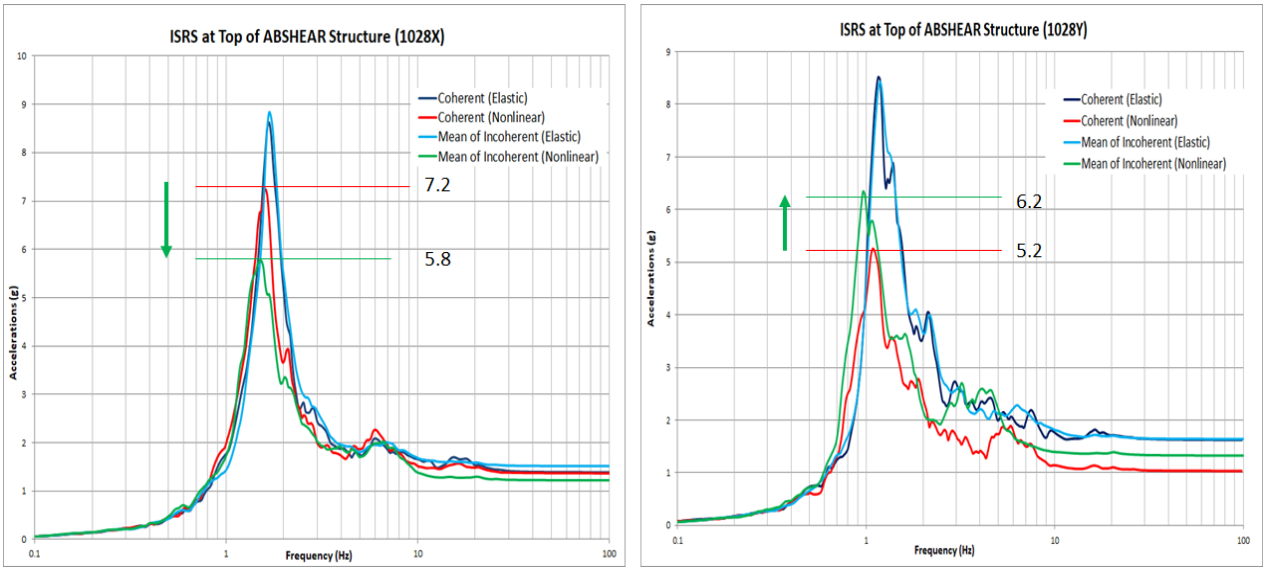

Figure 20 Linear and Nonlinear ISRS at AB Roof Corner Under Coherent and Incoherent Motions

The significant increase of the global torsional motion under incoherent motion is also shown in Figure 21 in terms of displacement responses. Figure 21 shows that the computed transverse displacements at two AB roof corners at the transverse building edges (on the left at node 33Y and on the right at node 1028Y in Figure 1). The AB structure corner transverse displacement amplitudes are much larger for the incoherent

motion, about twice larger. Also, the AB structure torsional rotation computed by the difference between the two lateral edge node displacements indicates that for the coherent motion.

The AB rotation is obtained by the difference between the blue and red lines, while for the incoherent motion is given by the difference between the green and magenta lines. There is a much larger torsional rotation for the incoherent motion, more than twice larger.

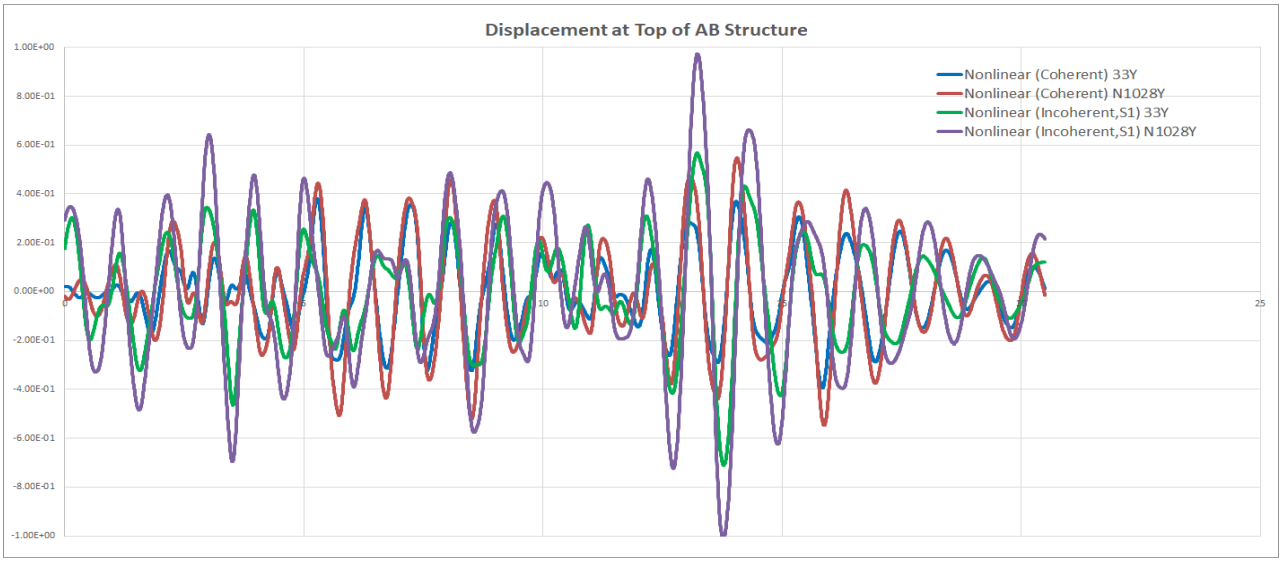

Figure 21 Seismic SSI Displacements AB Roof at Transverse Edges for Coherent and Incoherent Inputs

The motion incoherency differential displacement detrimental effects to the RC wall shear forces is shown in Figure 22 which shows the nonlinear hysteretic shear force and bending responses in the most damaged transverse wall panel at the bottom floor level. The incoherent shear forces and bending moments in the RC wall are much larger for the three stochastically simulated incoherent wave fields than for the coherent wave field. The three incoherent space-time wave field were simulated using ACS SASSI software via the Monte Carlo stochastic simulation for the Chiba site coherence functions.

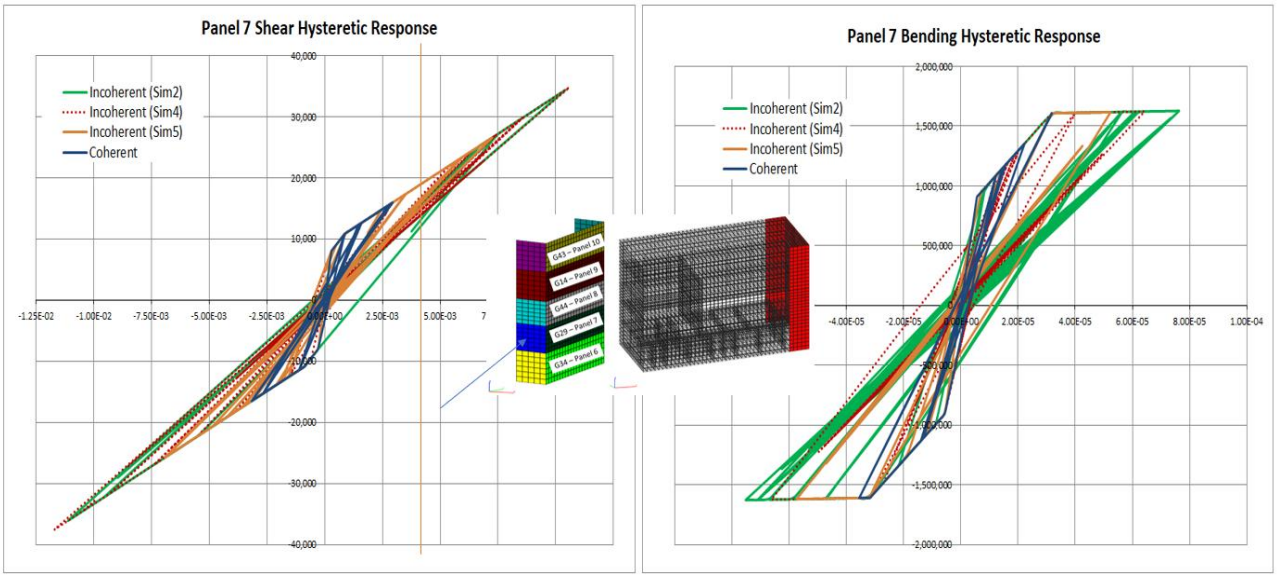

Figure 22 Incoherent vs. Coherent Shear Forces and Bending Moments in Transverse RC Wall at 1st Floor

This study results suggests a conceptual pitfall that exists in the traditional seismic design of structures. The kinematic SSI effects which are typically neglected in the seismic structure design could impact severely in certain, unfortunate situations of structures with significant mass eccentricities and large-size foundations under spatially varying seismic incoherent waves.

5. CONCLUDING REMARKS

The paper investigates the seismic SSI effects for a typical Auxiliary Building (AB) shearwall surface structure founded on a soft soil deposit subjected to severe coherent and incoherent seismic soil motions. The comparative results indicate that incoherent motions produce larger RC wall stress-dependent stiffness degradations than coherent motions. This is produced by the significant incoherent-induced kinematic SSI effects due to the incoherent, non-vertically propagating seismic waves, producing differential soil motions that increase the foundation bending deformation and stresses.

This study results suggest a conceptual pitfall in the traditional seismic design of structures. The structural design codes which are based on the ultimate state limit for the RC structures which does not include the structure support deformation effects. This is a potential engineering pitfall as shown in next section. The kinematic SSI effects due to the seismic wave soil differential motions are usually neglected, although they could impact severely on SSI structure responses in certain situations, such as for structures with significant mass eccentricities and/or with large-size foundation mats under spatially varying seismic or incoherent waves.

It should be noted that such differential soil motion effects are overlooked in seismic standards, most-likely due to the foundation rigid-body assumption (assuming there is no foundation deformability), but not overlooked for the multiple support structures, such as bridges, or nuclear piping and multipoint supported equipment systems assumed with a flexible foundation. These effects are larger for soft soil deposits and large-size foundations for which the non-vertically propagating incident seismic wave wavelengths could be only a fraction of the foundation sizes.

6. REFERENCES

Ghiocel, D.M, Nitta, Y., Ikeda, R. and Shono, T (2022a, 2022b). *Seismic Nonlinear SSI Approach Based on Best Practices in US and Japan. Parts 1: Modeling and Part 2: Application*, SMiRT26, Special Session, Berlin, July 10-15

GP Technologies (2023) *ACS SASSI NQA Version 4.3.6 - An Advanced Computational Software for 3D Dynamic Analysis Including Soil-Structure Interaction, Including Options A-AA and NON Advanced,* GP Technologies, Inc., User Manuals, Revision 8, New York, USA

Ichihara, Y., Nakamura, N, Nabeshima, K., Choi, B. and Nishida, A. (2022). *Applicability of Equivalent Linear Three-Dimensional FEM Analysis for Reactor Building to Seismic Response of SSI System*, SMiRT26 Conference, Special Session on Nonlinear Seismic SSI Analysis Based on Best Practices in US and Japan, Berlin, July 10-15

JEAC 4016-2015, Nuclear Standard Committee of Japan Electric Association (2015), *Technical Code for Aseismic Design of Nuclear Power Plants*, *Japan Electric Association*

Nitta, Y., Ikeda, R., Horiguchi, T. and Ghiocel, D.M. (2022). *Comparative Study Using Stick and 3DFEM Nonlinear SSI Models per JEAC 4601-2015 Recommendations*, SMiRT26, Special Session on Nonlinear Seismic SSI Analysis Based on Practices in US and Japan, July 10-15